Modified Numerical Scheme for Perona-Malik Model in Image Restoration

Zhiyi Ruan, Youjian Shen(✉), and Fengling Liu

College of Mathematics and Statistics, Hainan Normal University,
No. 99 Longkun South Road, Haikou 571158, China
{fafurzy,flliu116}@163.com, yjshen678@qq.com

Abstract. This paper proposes a difference scheme based on nonlinear diffusion Perona-Malik model for numerical calculation in image restoration. Our scheme can adapt to determine the tangent directions to the isophote lines based on two mutually orthogonal directional derivatives, which results that diffusion is along the edges as much as possible. One of typical edge stopping functions for Perona-Malik model is modified in order to improve robust calculation and satisfy the compatibility, stability and convergence for our numerical scheme. Computer experimental results indicate that the algorithm corresponding to our numerical scheme is very efficient for noise removal in regardless whether the noise is serious or not.

Keywords: Image restoration · Difference scheme · Numerical calculation · Perona-Malik model · Nonlinear diffusion

1 Introduction

Historically, image restoration is not only one of the oldest concerns but also one of the most important and fundamental tasks [1]. Removing the noise while preserving image edges is difficult but much desired. Nowadays, for this aim there emerge three main directions: stochastic modeling, wavelets and partial differential equation (PDE) approaches [2][3].

For PDE-based methods, Perona-Malik (P-M) model (ref. [4]) is considered to be the most classic equation so that it has attracted much attention in recent decades; see [5], [6] and [7], etc. However, P-M model is pathological [5][8]. In other words, robust calculation of diffusion coefficient is a severe challenge for the model when the noise of the initial image is sharp oscillation. A classical method to overcome this disadvantage is the smooth version of P-M model proposed by Catté et al. in [5]. As two-dimensional Gaussian kernel G_σ is introduced into edge stopping function, their model can smooth the flat and edge regions adaptively. However, it's difficult to choose proper scale parameter σ. In order to further improve the cases depending seriously on the gradient values of an image, Guo et al. proposed an adaptive P-M model by variable exponent term $|\nabla u|^{\alpha(|\nabla G_\sigma * u|^2)}$ (Edge indicator function must satisfy $0 \leq \alpha(\cdot) \leq 2$.) replacing

H. Zha et al. (Eds.): CCCV 2015, Part I, CCIS 546, pp. 366–375, 2015.
DOI: 10.1007/978-3-662-48558-3_37

$|\nabla u|^2$ for edge stopping function in [7]. When the model is applied to image processing, experimental results show that it can achieve higher quality images for peak signal to noise ratio (PSNR) and image edge has been preserved better. A similar model was mentioned by Maiseli et al. [9] with different edge indicator function from [7].

This paper improves robust calculation of P-M model by modifying one of typical edge stopping functions. Meanwhile, we present a new numerical scheme for P-M model. P-M model is recalled in Sect. 2.1 and our scheme is deduced from the aspect of numerical analysis in Sect. 2.2. According to the product of two mutually orthogonal directional derivatives is negative or not, we give two distinct second-order mixed partial derivatives. The form of our difference equation makes diffusion along the edges (the isophote lines) as much as possible. Thus, our scheme neither has very strong isotropic smoothing properties like heat equation nor restores images only depending on the difference of gray level value among different pixels. After proving the compatibility, stability and convergence of the difference equation (Sect. 2.3), Sect. 3 makes use of Lena image and Cameraman image added Gaussian noise for different variances to test the capability of our new scheme in image restoration. Compared with those models proposed by [4], [5] and [7], experimental results show that our algorithm has significant advantages. Conclusion is in Sect. 4.

2 Nonlinear Diffusion in Image Restoration

In image processing, the oldest and most investigated equation is probably the parabolic linear heat equation [10][11]. Although it has successful applications, there exists a drawback that it is too smoothing so that edges will be lost, i.e., image becomes severely blurred after being processed. Many researchers have tried to find more effective models or algorithms for removing the noise while preserving the edge as much as possible [1].

2.1 Perona-Malik Model

In [4], Perona and Malik proposed anisotropic diffusion equation as follows

$$u_t = div(c(|\nabla u|^2)\nabla u),\ u(x, y, 0) = u_0(x, y), \tag{1}$$

which is called P-M model, where u_0 is initial image and edge stopping function $c(\cdot)$ is strictly monotonically decreasing function satisfying $c(0) = 1$, $c(s) \geq 0$ and $c(s) \to 0$ as $s \to +\infty$. In addition, denoting respectively by div and ∇ the divergence operator and the gradient operator (i.e., $\nabla u = (u_x, u_y)$ and $|\nabla u|^2 = u_x^2 + u_y^2$) with respect to the space variables (x, y).

After researching experiment, there are two edge stopping functions adopted widely, i.e., $c(s) = (1 + s/K)^{-1}$ and $c(s) = exp(-s/K)$, where K is a positive constant. For the former, we will investigate further the function $c(s) = (1 + s/K)^{-1/3}$ in improving robust calculation of P-M model.

On the one hand, in flat areas P-M model acts as the heat equation which is isotropic smoothing since c approximates to a constant as the value of the gradient is almost equal to zero. On the other hand, its regularization near the region's boundaries is weaken even stopped such that the edge are preserved.

According to the definition of divergence operator, (1) can be written as the form of second-order partial derivatives in spatial directions, i.e.,

$$\frac{\partial u}{\partial t} = c_{11}(\nabla u) \cdot u_{xx} + 2c_{12}(\nabla u) \cdot u_{xy} + c_{22}(\nabla u) \cdot u_{yy}, \tag{2}$$

where diffusion coefficients satisfy

$$\begin{cases} c_{11}(\nabla u) = 2u_x^2 c'(|\nabla u|^2) + c(|\nabla u|^2), \\ c_{12}(\nabla u) = 2u_x u_y c'(|\nabla u|^2), \\ c_{22}(\nabla u) = 2u_y^2 c'(|\nabla u|^2) + c(|\nabla u|^2). \end{cases}$$

To facilitate the writing, in the back content $c_{11}(\nabla u)$, $c_{12}(\nabla u)$, and $c_{22}(\nabla u)$ is abbreviated as c_{11}, c_{12}, and c_{22}, respectively.

2.2 Modified Numerical Scheme

As a matter of fact, a stable 4-nearest-neighbors discretization of Laplacian operator given by [4] for P-M model is weaken even almost stopped when the value of $|\nabla u|$ is tremendous. In such a case, the edge are protected, but noise on the edge is still retained. On the one hand, if the noise of the initial image u_0 is sharp oscillations, P-M model will face a severe challenge which is how to calculate robustly the diffusion coefficients c from the outset. On the other hand, it's difficult to identify the true boundary or "boundary" caused by noise. Unfortunately, P-M model with the 4-nearest-neighbors discretization of Laplacian operator can't exhibit theoretically expected effect in practical applications.

Finite difference method is utilized for the discretization of partial derivatives since digital image has a natural regular grid. In this Section, we will transform P-M model into an explicit difference scheme for the numerical calculation. In terms of (2), the differential quotients with respect to the spatial variables (x, y) are approximated by center difference quotients and the differential quotient with respect to the temporal variable t is approximated by forward difference quotient in this paper.

Introduce the time step size Δt and the spatial step sizes Δx, Δy into difference equation, i.e., $t = n \cdot \Delta t$, $x = i \cdot \Delta x$ and $y = j \cdot \Delta y$. It follows that

$$\begin{aligned} &\left(\frac{\partial u}{\partial t}\right)^n = \frac{u^{n+1} - u^n}{\Delta t}, \left(\frac{\partial u}{\partial x}\right)_{i,j} = \frac{u_{i+1,j} - u_{i-1,j}}{2\Delta x}, \left(\frac{\partial u}{\partial y}\right)_{i,j} = \frac{u_{i,j+1} - u_{i,j-1}}{2\Delta y}, \\ &\left(\frac{\partial^2 u}{\partial x^2}\right)_{i,j} = \frac{u_{i+1,j} - 2u_{i,j} + u_{i-1,j}}{(\Delta x)^2}, \left(\frac{\partial^2 u}{\partial y^2}\right)_{i,j} = \frac{u_{i,j+1} - 2u_{i,j} + u_{i,j-1}}{(\Delta y)^2}. \end{aligned} \tag{3}$$

It is necessary to point out that the difference quotient of second-order mixed partial derivative used commonly (e.g., given in [12]):

$$\left(\frac{\partial^2 u}{\partial x \partial y}\right)_{i,j} = \frac{u_{i+1,j+1} - u_{i+1,j-1} - u_{i-1,j+1} + u_{i-1,j-1}}{4\Delta x \Delta y}$$

couldn't make sure of the stability and convergence of the corresponding difference scheme in iterative procedure. Considering the coefficients of $u_{i+1,j+1}$, $u_{i+1,j-1}$, $u_{i-1,j+1}$ and $u_{i-1,j-1}$ in the difference quotient mentioned as above, half are negative and half are positive. Furthermore, the righthand coefficients of (2) rely strictly upon two mutually orthogonal directional derivatives in numerically. Therefore, this difference equation doesn't satisfy the maximum principle.

Without loss of generality, we set $k = \Delta t$ and $h = \Delta x = \Delta y$. As $h \to 0$, let's consider Taylor Expansions of four terms $u_{i+1,j+1}$, $u_{i+1,j-1}$, $u_{i-1,j+1}$ and $u_{i-1,j-1}$ at point (i, j), i.e.,

$$u_{i+1,j+1} = \left[1 + h\left(\frac{\partial}{\partial x} + \frac{\partial}{\partial y}\right) + \frac{h^2}{2}\left(\frac{\partial}{\partial x} + \frac{\partial}{\partial y}\right)^2 + \frac{h^3}{6}\left(\frac{\partial}{\partial x} + \frac{\partial}{\partial y}\right)^3\right] u_{i,j}, \quad (4)$$

$$u_{i+1,j-1} = \left[1 + h\left(\frac{\partial}{\partial x} - \frac{\partial}{\partial y}\right) + \frac{h^2}{2}\left(\frac{\partial}{\partial x} - \frac{\partial}{\partial y}\right)^2 + \frac{h^3}{6}\left(\frac{\partial}{\partial x} - \frac{\partial}{\partial y}\right)^3\right] u_{i,j}, \quad (5)$$

$$u_{i-1,j+1} = \left[1 - h\left(\frac{\partial}{\partial x} - \frac{\partial}{\partial y}\right) + \frac{h^2}{2}\left(\frac{\partial}{\partial x} - \frac{\partial}{\partial y}\right)^2 - \frac{h^3}{6}\left(\frac{\partial}{\partial x} - \frac{\partial}{\partial y}\right)^3\right] u_{i,j}, \quad (6)$$

$$u_{i-1,j-1} = \left[1 - h\left(\frac{\partial}{\partial x} + \frac{\partial}{\partial y}\right) + \frac{h^2}{2}\left(\frac{\partial}{\partial x} + \frac{\partial}{\partial y}\right)^2 - \frac{h^3}{6}\left(\frac{\partial}{\partial x} + \frac{\partial}{\partial y}\right)^3\right] u_{i,j}, \quad (7)$$

where all of remainders are $\mathcal{O}(h^4)$. To eliminate first-order partial derivatives, let (5) add (6) and (4) add (7). Therefore, we deduce the following two equations with respect to second-order mixed partial derivative:

$$2\left(\frac{\partial^2 u}{\partial x \partial y}\right)_{i,j} = \frac{2u_{i,j} - u_{i+1,j-1} - u_{i-1,j+1}}{h^2} + \left(\frac{\partial^2 u}{\partial x^2} + \frac{\partial^2 u}{\partial y^2}\right)_{i,j} + \mathcal{O}(h^2), \quad (8)$$

$$2\left(\frac{\partial^2 u}{\partial x \partial y}\right)_{i,j} = \frac{u_{i+1,j+1} + u_{i-1,j-1} - 2u_{i,j}}{h^2} - \left(\frac{\partial^2 u}{\partial x^2} + \frac{\partial^2 u}{\partial y^2}\right)_{i,j} + \mathcal{O}(h^2). \quad (9)$$

For the discrete approximation of u_{xy} in (2), we choose to apply (8) if coefficient c_{12} is negative, and (9) if c_{12} is nonnegative. Our choices can fundamentally avoid the divergent and unstable result caused from the case mentioned as above for the difference form given by [12]. In addition, it's possible to result in appearing negative coefficients for other terms (for example, $u_{i,j}$, $u_{i+1,j}$ and $u_{i,j-1}$, etc). However, we only require some appropriate constraints for this.

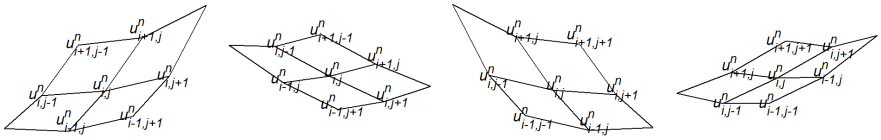

(a) $u_x > 0, u_y > 0$ (b) $u_x < 0, u_y < 0$ (c) $u_x > 0, u_y < 0$ (d) $u_x < 0, u_y > 0$

Fig. 1. Illustration of Difference Equation (10)

In such choices, we obtain the following Difference Equation of P-M model by (3), (8) and (9):

$$u_{i,j}^{n+1} = \begin{cases} C_1 u_{i,j}^n + C_2 u_{i+1,j}^n + C_2 u_{i-1,j}^n + C_3 u_{i,j+1}^n \\ \qquad + C_3 u_{i,j-1}^n + C_4 u_{i+1,j-1}^n + C_4 u_{i-1,j+1}^n, & \text{if } c_{12} < 0 \\ C_1 u_{i,j}^n + C_2 u_{i+1,j}^n + C_2 u_{i-1,j}^n + C_3 u_{i,j+1}^n \\ \qquad + C_3 u_{i,j-1}^n + C_4 u_{i+1,j+1}^n + C_4 u_{i-1,j-1}^n, & \text{if } c_{12} \geq 0 \end{cases} \tag{10}$$

where

$$\begin{cases} C_1 = 1 - 2rc_{11} - 2rc_{22} + 2r|c_{12}|, \\ C_2 = r(c_{11} - |c_{12}|), \\ C_3 = r(c_{22} - |c_{12}|), \\ C_4 = r|c_{12}|, \end{cases}$$

where $r = k/h^2$. There is no doubt that ideal initial values are original degraded noisy images. As shown in Fig. 1, it's not hard to see that the diffusion form is related closely with the tangent directions to the isophote lines in image.

2.3 Compatibility, Stability and Convergence

Theorem 1. *Difference Equation (10) is compatible with (2).*

Proof. Firstly, we prove the theorem in the case $c_{12} < 0$. We obtain local truncation error of (10) as follows

$$\begin{aligned} T_{i,j}^n = & \left[\frac{u_{i,j}^{n+1} - u_{i,j}^n}{k} - |c_{12}| \frac{u_{i+1,j-1}^n + u_{i-1,j+1}^n - 2u_{i,j}^n}{h^2} \right. \\ & \left. - (c_{11} - |c_{12}|) \frac{u_{i+1,j}^n + u_{i-1,j}^n - 2u_{i,j}^n}{h^2} - (c_{22} - |c_{12}|) \frac{u_{i,j+1}^n + u_{i,j-1}^n - 2u_{i,j}^n}{h^2} \right] \\ & - \left[\frac{\partial u}{\partial t} - \left(c_{11} \frac{\partial^2 u}{\partial x^2} + 2c_{12} \frac{\partial^2 u}{\partial x \partial y} + c_{22} \frac{\partial^2 u}{\partial y^2} \right) \right]_{i,j}^n . \end{aligned}$$

As $k \to 0$ and $h \to 0$, we have Taylor Expansions of the righthand terms $u_{i,j}^{n+1}$, $u_{i+1,j}^n$ and $u_{i-1,j+1}^n$, etc. in (10) at point (i, j, n). Then, it is easy to deduce that $T_{i,j}^n = \mathcal{O}(k + h^2) \to 0$.

For the case $c_{12} \geq 0$, the same result can be obtained similarly. Consequently, we conclude that (10) is compatible with (2). □

Theorem 2. *For $c(s) = (1 + s/K)^{-p}$ $(0 < p \leq 1/3)$, Difference Equation (10) is stable if $r \leq 1/4$.*

Proof. It's apparent from (10) that the sum of the righthand coefficients C_i $(i = 1, \cdots, 4)$ is equal to 1. Firstly, we will prove that every coefficient is nonnegative, i.e.,

$$\begin{cases} 1 - 4r\big[\big(u_x^2 + u_y^2 + |u_x u_y|\big)c'(|\nabla u|^2) + c(|\nabla u|^2)\big] \geq 0, \\ r\big[2\big(max\{u_x^2, u_y^2\} + |u_x u_y|\big)c'(|\nabla u|^2) + c(|\nabla u|^2)\big] \geq 0, \\ -2r|u_x u_y|c'(|\nabla u|^2) \geq 0. \end{cases} \tag{11}$$

In fact, according to the monotonicity of edge stopping function $c(\cdot)$, the last inequality of (11) is naturally true because both the time and spatial step size are positive constants. Next, let's prove the second inequality of (11). It is straightforward to show that

$$2(max\{u_x^2, u_y^2\} + |u_x u_y|) \leq 2(u_x^2 + u_y^2) + (u_x^2 + u_y^2) = 3|\nabla u|^2.$$

By differentiating the function $c(s) = (1 + s/K)^{-p}$ with respect to s, we can get

$$c'(s) = -\frac{p/K}{(1 + s/K)^{p+1}} = -\frac{p/K}{1 + s/K}c(s).$$

For $p \leq 1/3$, we can deduce

$$2\big(max\{u_x^2, u_y^2\} + |u_x u_y|\big)c'(|\nabla u|^2) + c(|\nabla u|^2) \geq 0.$$

Similarly, in terms of the first inequality, we can easily obtain

$$0 \leq \big(u_x^2 + u_y^2 + |u_x u_y|\big)c'(|\nabla u|^2) + c(|\nabla u|^2) \leq 1.$$

So the first inequality of (11) is true if $r \leq 1/4$.

Denoting by u_{max}^0 and u_{min}^0 the maximum and minimum of initial values respectively. In fact, we can obtain

$$u_{min}^0 \leq u_{i,j}^n \leq u_{max}^0$$

for every (i, j, n) by means of the maximum principle. More generally, for each positive integer n there exists a positive constant P such that

$$\|u^n\| \leq P\|u^0\|,$$

where the norm $\|u\| = \big[\sum_{i,j}(u_{i,j})^2\big]^{\frac{1}{2}}$. Combined this with Theorem 1, the conclusion is proved. □

Therefore, all values always remain boundedness in the whole iterative procedure. In fact, as has been proved in Theorem 2, the gray level value of all pixels will tend to some constant with increasing of iteration count. In general, it is a common drawback for the explicit difference scheme. Thus, we need to control the number of iterations to avoid blurring the image.

Since (10) is linear, we obtain the following theorem (ref. [13]):

Theorem 3. *Under Theorem 1, stability of Difference Equation (10) is a necessary and sufficient condition that it be convergent.*

3 Numerical Comparison

In this Section, we will compare the denoising effect of the algorithm for our numerical scheme with the algorithms for P-M model [4], Catté-Lions-Morel-Coll (C-L-M-C) model [5] and Guo-Sun-Zhang-Wu (G-S-Z-W) model [7] which are programmed by 4-nearest-neighbors discretization of Laplacian operator. These denoising algorithms are tested on standard Lena image (see Fig. 2(a)), Cameraman image (see Fig. 2(b)) and the versions added Gaussian noise for different variances. Gray level value of each pixel is an integer from 0 to 255.

(a) Lena (b) Cameraman

Fig. 2. The standard images (512×512 pixels)

PSNR which is applied to evaluate the quality of the restored images in this paper is defined as

$$PSNR = 10 \times \log\left(\frac{255^2}{MSE}\right),$$

where MSE (mean square error) is defined as

$$MSE = \frac{\sum_{j=1}^{N}\sum_{i=1}^{M}\left[u_{i,j} - (u_0)_{i,j}\right]^2}{M \times N},$$

where M and N represent respectively the number of image pixels in rows and columns. All algorithms are run in Matlab R2008a on a Pentium(R) Dual-Core CPU T4300 @ 2.10GHz processor. In addition, the iterative stopping criterion of all algorithms is set to acquire the maximal PSNR.

First noisy observation is generated by adding the Gaussian white noise for mean $\mu = 0$ and standard deviation $\sigma = 25$ into Lena image ($PSNR = 22.6017$, see Fig. 3(a)). All parameters used in these denoising algorithms are shown in the title of Fig. 3 ($r = 0.1$, $c_1(s) = (1+s)^{-1/3}$ and $c_2(s) = (1+s/32)^{-1}$). The denoising effect is shown in Fig. 3(b)-3(f). PSNR and iteration count are seen in Table 1.

As can be seen from Table 1, PSNR and iteration count of the algorithm corresponding to our scheme is essentially flat with the algorithms for C-L-M-C model and G-S-Z-W model. For the 4-nearest-neighbors discretization of P-M model, $c_2(s)$ performs worse than $c_1(s)$ and becomes the worst by lowest PSNR and largest iteration count. Judging from this, the function $c(s) = (1+s/K)^{-1/3}$

(a) (b) (c) (d) (e) (f)

Fig. 3. Lena image. (a) Noise image corrupted by Gaussian noise for $\sigma = 25$; (b) Our algorithm with $c_1(s)$; (c) P-M model with $c_1(s)$; (d) P-M model with $c_2(s)$; (e) C-L-M-C model with $c_2(s)$, $\sigma = 0.5$ for Gaussian kernel; (f) G-S-Z-W model with $c_2(s)$, $\sigma = 0.5$ for Gaussian kernel and $k = 0.5$ for variable exponent coefficient.

Table 1. PSNR (dB) and iteration count (steps) for Fig. 3

	(b)	(c)	(d)	(e)	(f)
PSNR	33.7858	33.4970	31.7632	33.6233	33.6192
Iteration count	84	69	192	94	90

(a) (b) (c) (d) (e) (f)

Fig. 4. Lena image. (a) Noise image corrupted by Gaussian noise for $\sigma = 100$; (b) Our algorithm with $c_1(s)$; (c) P-M model with $c_1(s)$; (d) P-M model with $c_2(s)$; (e) C-L-M-C model with $c_2(s)$, $\sigma = 1.5$ for Gaussian kernel; (f) G-S-Z-W model with $c_2(s)$, $\sigma = 1.5$ for Gaussian kernel and $k = 1$ for variable exponent coefficient.

Table 2. PSNR (dB) and iteration count (steps) for Fig. 4

	(b)	(c)	(d)	(e)	(f)
PSNR	25.1603	23.8122	22.9253	23.9372	23.9288
Iteration count	288	208	1331	192	188

is more beneficial for calculating robustly of P-M model than typical function $c(s) = (1 + s/K)^{-1}$.

Second noisy observation is generated by adding the Gaussian white noise for mean $\mu = 0$ and standard deviation $\sigma = 100$ into Lena image ($PSNR = 12.5610$, see Fig. 4(a)). All parameters used in these denoising algorithms are shown in the title of Fig. 4 ($r = 0.1$, $c_1(s) = (1 + s)^{-1/3}$ and $c_2(s) = (1 + s/32)^{-1}$). The denoising effect is shown in Fig. 4(b)-4(f). PSNR and iteration count are seen in Table 2.

Last noisy observation is generated by adding the Gaussian white noise for mean $\mu = 0$ and standard deviation $\sigma = 100$ into Cameraman image ($PSNR =$

13.1543, see Fig. 5(a)). All parameters used in these denoising algorithms are shown in the title of Fig. 5 ($r = 0.2$, $c_1(s) = (1+s)^{-1/3}$ and $c_2(s) = (1+s/16)^{-1}$). The denoising effect is shown in Fig. 5(b)-5(f). PSNR and iteration count are seen in Table 3.

(a) (b) (c) (d) (e) (f)

Fig. 5. Cameraman image. (a) Noise image corrupted by Gaussian noise for $\sigma = 100$; (b) Our algorithm with $c_1(s)$; (c) P-M model with $c_1(s)$; (d) P-M model with $c_2(s)$; (e) C-L-M-C model with $c_2(s)$, $\sigma = 1.5$ for Gaussian kernel; (f) G-S-Z-W model with $c_2(s)$, $\sigma = 1.5$ for Gaussian kernel and $k = 1$ for variable exponent coefficient.

Table 3. PSNR (dB) and iteration count (steps) for Fig. 5

	(b)	(c)	(d)	(e)	(f)
PSNR	23.1283	21.9037	21.2401	22.1715	22.1549
Iteration count	141	104	1292	147	144

Obviously, ours performs best in these denoising algorithms according to the comparison data seen in Table 2 and 3 in spite of being added more noise. And the experimental results have almost no difference among the algorithms for P-M model with $c_1(s)$, C-L-M-C model and G-S-Z-W model with $c_2(s)$. The denoising effect of P-M model with $c_2(s)$ is still the worst. This indicates again that $c(s) = (1 + s/K)^{-1/3}$ is indeed conducive to improve robust calculation of P-M model.

4 Conclusion

This paper proposes a modified numerical scheme based on nonlinear diffusion P-M model in image restoration. Our new scheme not only has isotropic smoothing properties acting as heat equation, but can calculate the diffusion intensity relying on the gradient value of gray image like P-M model. Furthermore, it also can determine adaptively the diffusion directions according to the gray level value of pixels in images. Judging from experimental results, our algorithm is more effective in achieving the purpose of diffusing along the edges than the algorithms for P-M model etc. which are programmed by 4-nearest-neighbors discretization of Laplacian operator. Meanwhile, in terms of calculating robustly, the function $c(s) = (1 + s/K)^{-1/3}$ is more suitable to be adopted for P-M model.

Acknowledgments. The authors would like to thank the National Natural Science Foundation of China (Grant No. 11461018) and the Postgraduate Innovative Research Project of Hainan Province in China (Grant No. Hys2014-55).

References

1. Aubert, G., Kornprobst, P.: Mathematical Problems in Image Processing: Partial Differential Equations and the Calculus of Variations. Applied Mathematical Sciences. Springer, New York (2002)
2. Chan, T.F., Shen, J.: Image Processing and Analysis: Variational, PDE, Wavelet, and Stochastic Methods. SIAM, Philadelphia (2005)
3. Aubert, G., Kornprobst, P.: Mathematics of Image Processing. Encyclopedia of Mathematical Physics **3**, 1–9 (2006)
4. Perona, P., Malik, J.: Scale-space and Edge Detection using Anisotropic Diffusion. IEEE Transactions on Pattern Analysis and Machine Intelligence **12**(7), 629–639 (1990)
5. Catté, F., Lions, P.L., Morel, J.M., et al.: Image Selective Smoothing and Edge Detection by Nonlinear Diffusion. SIAM Journal of Numerical Analysis **29**, 182–193 (1992)
6. Colombo, M., Gobbino, M.: Slow Time Behavior of the Semidiscrete Perona-Malik Scheme in One Dimension. SIAM Journal of Mathematical Analysis **43**(6), 2564–2600 (2011)
7. Guo, Z., Sun, J., Zhang, D., et al.: Adaptive Perona-Malik Model Based on the Variable Exponent for Image Denoising. IEEE Transactions on Image Processing **21**(3), 958–967 (2012)
8. Kichenassamy, S.: The Perona-Malik paradox. SIAM Journal of Applied Mathematics **57**(5), 1328–1342 (1997)
9. Maiseli, B., Elisha, O., Mei, J., et al.: Edge Preservation Image Enlargement and Enhancement Method Based on the Adaptive Perona-Malik Non-linear Diffusion Model. IET Image Processing **8**(12), 753–760 (2014)
10. Koenderink, J.J.: The Structure of Images. Biological Cybernetics **50**, 363–370 (1984)
11. ter Bart, M.: Haar Romeny: Geometry-driven Diffusion in Computer Vision. Computational Imaging and Vision. Kluwer Academic Publishers, Dordrecht (1994)
12. Xiao, Z., Xu, Z., Zhang, F., et al.: ESPI Filtering Method Based on Anisotropic coherence Diffusion and Perona-Malik Diffusion. Chinese Optics Letters **11**, 101101-1–101101-4 (2013)
13. Lax, P.D., Richtmyer, R.D.: Survey of the Stability of Linear Finite Difference Equations. Connumcarrons on Pure and Applied Mathematics **ix**, 267–293 (1956)